Polymer Degradation and Stability 191 (2021) 109670

Contents lists available at ScienceDirect

Polymer Degradation and Stability

journal homepage: www.elsevier.com/locate/polymdegradstab

Water absorption and hydrothermal ageing of epoxy adhesives reinforced with amino-functionalized graphene oxide nanoparticles

Olesja Starkova[a,*], Sergejs Gaidukovs[b], Oskars Platnieks[b], Anda Barkane[b], Kristina Garkusina[c], Eriks Palitis[c], Liga Grase[d]

[a] Institute for Mechanics of Materials, University of Latvia, Jelgavas 3, LV-1004 Riga, Latvia
[b] Institute of Polymer Materials, Faculty of Materials Science and Applied Chemistry, Riga Technical University, P. Valdena 3/7, LV-1048 Riga, Latvia
[c] Institute of Applied Chemistry, Faculty of Materials Science and Applied Chemistry, Riga Technical University, P. Valdena 3/7, LV-1048 Riga, Latvia
[d] Institute of Silicate Materials, Faculty of Materials Science and Applied Chemistry, Riga Technical University, P. Valdena 3/7, LV, 1048 Riga, Latvia

ARTICLE INFO

Article history:
Received 2 March 2021
Revised 27 May 2021
Accepted 4 July 2021
Available online 7 July 2021

Keywords:
Amine cured epoxy
Graphene oxide nanoparticles
Non-Fickian diffusion
Leaching, modelling
FTIR
Dynamic mechanical analysis
Reinforcing efficiency
Degradation
Plasticization

ABSTRACT

The study is focused on quantitative characterization of water absorption and hydrothermal ageing effects in a room-temperature amine cured epoxy adhesive widely used in automotive, aerospace, construction, and marine industries. Amino-functionalized graphene oxide (mGO) nanoparticles were incorporated into the epoxy (up to 1.72 wt.%) enabled cross-linking reactions and providing high interfacial adhesion, superior reinforcement efficiency and enhanced resistance to hydrothermal ageing of nanocomposites. Anomalous water absorption accompanied by progressive weight loss of samples (down to 7%) is fitted by two-stage models considering additive and coupled contribution from water diffusion and leaching of low molecular weight epoxy species. Nanocomposites are characterized by lower water diffusivity (40%) and decreased leaching effects (70%). High reinforcing efficiency of epoxy/mGO appeared in the increased glassy and rubbery storage moduli (60%), glass transition temperature (10 °C) and activation energy of glass transition (70%) compared to the neat epoxy. Hydrothermal ageing resulted in noticeable properties degradation of samples, although to a much lower extent in the case of nanocomposites. The results will contribute to the enhancement of global durability of common epoxy-based adhesives and extension of their lifetime.

1. Introduction

Epoxy adhesives are the most extensively used engineering adhesives owing to their excellent mechanical performance and adhesion to various substrates, e.g. metals, ceramics, glass, concrete, wood and plastics, and used in diverse applications ranging from general industry to electronics, construction, automotive, aerospace and marine industries [1–4]. Properties of the epoxy depend on the amount of crosslinking as well as the structure of used components. The hardener part of the epoxy system often introduces hydrophilic sites in the structure and is sensitive to humidity [5]. The use of relatively small amounts of nanoparticles as additives allows one to significantly influence material properties and reduce water impact. 2D nanoparticles, e.g. graphene and graphene oxide (GO) nanoplatelets, are among the most promising candidates for enhancing barrier properties and environmental durability of epoxies [3,6,7].

Hydrothermal ageing [2,3,6–9] for epoxy systems can be reversible if caused by water-induced plasticization effects or irreversible when related to chemical changes like thermo-oxidation, hydrolysis, cracking due to swelling and embrittlement during post-curing or physical ageing. The degree of hygrothermal degradation and lifetime of epoxy adhesives depend on operating temperature. Degradation of amine-based epoxies is mostly reversible at temperatures below glass transition temperature (T_g), and properties are recovered as soon as absorbed water is removed from the polymer. Under elevated temperature, secondary irreversible degradation mechanisms could be activated [10,11]. For example, hydrolysis and thermo-oxidation alter the cohesive mechanics of the molecular network, its hydrophilicity and result in significant changes in water transport properties [9,12–15]. Hydrolysis is commonly observed in anhydride-cured epoxy systems [13,14], although this could also present in amine epoxies under specific conditions of remained non-reacted epoxy groups and in non-ideal networks [11]. Deterioration of the molecular structure causes progressive loss in mechanical properties. At the same time, absorbed water beside its plasticization effect could promote ad-

* Corresponding author.
E-mail address: olesja.starkova@lu.lv (O. Starkova).

https://doi.org/10.1016/j.polymdegradstab.2021.109670
0141-3910/

ditional crosslinking by post-curing and physical ageing counterbalancing in that way negative environmental impact [7,8,16–18]. These effects are usually found in thermosets cured at low temperatures like two-component systems for basic engineering applications [2,8]. Understanding the mechanisms of properties degradation, evaluation of their additive or competitive contribution is crucial for the development of reliable methods for the prediction of long-term service performance and lifetime of epoxy-based adhesives, coatings, and composites.

The long-term performance estimations for materials exploited in the humid environment are commonly related to the amount of absorbed water and T_g changes known as the determining parameters in some of the accelerated testing methods [15,16]. The water sorption capacity, i.e. the equilibrium water content of samples, is usually determined by simple gravimetric measurements. However, interpretation of gravimetric data becomes challenging, when water uptake is accompanied by polymer relaxation and chemical decomposition processes [2,7,10–15,20]. The true water uptake process is masked by weight decrease due to leaching of low molecular weight species such as unreacted starting materials or hydrolysis products [12,13,15]. Depending on exposure temperature, the accompanying process can begin at different soaking durations after the immersion. It should also be mentioned that most of studies on water diffusion of epoxies considers model epoxy systems with perfectly known and controlled composition. However, industrial adhesives often have complex and heterogeneous composition due to mixture of various epoxy monomers, inorganic fillers, accelerators, plasticizers, solvents, etc. that could appear in non-classical water diffusion and complex hydrothermal ageing effects [21]. In polymer composites, severe deviations from the Fickian diffusion behaviour are usually accompanied by noticeable degradation due to irreversible physical or chemical damage of a polymer matrix and dissociation of a material located at the vicinities of particle/matrix or fibre/matrix interfaces [12,17,20,22]. Thus, assessment of weight changes of material during its service life is necessary for awareness of general durability issues. Also, the leaching of macromolecules from the polymer to external water is a major environmental concern [23]. Nanoparticles incorporated into polymers enhance their mechanical behaviour, chemical resistance, and thus, increase their lifetime [1]. Owing to the graphene's high aspect ratio providing tortuosity effect and restricted segmental motions of a polymer around the particle, graphene-based epoxies possess better barrier properties than the neat counterparts. This appears in lower diffusion rates and lower water absorption capacity of nanoparticles modified epoxies, which in turn contribute to the improved hydrothermal ageing resistance [3,6,7,24–27]. However, the positive impact of graphene on the properties' improvement is often far below the expected one. Poor dispersion, lack of interfacial adhesion between the polymer and filler could introduce defects in the structure leading to underwhelming results.

Functionalization of graphene has been widely adopted to improve its interfacial adhesion with the polymer and reduce particle agglomerations [28,29]. Ribeiro et al. reported that tetraethylenepentamine-modified GO improves the thermal properties of epoxy-based nanocomposites with best results at 0.5 wt.% loadings [30]. In a different study, Naebe and colleagues reported about the carboxyl group modified GO enhancing the dynamical mechanical and flexural properties of an epoxy resin [31]. Polyhedral oligomeric silsesquioxane modified graphene was reported as a potential additive to reduce epoxy corrosion [32]. Li et al. reported that the presence of modified GO facilitated the curing reaction, especially the initial epoxy-amine reaction [33]. Excellent UV resistance together with increased weathering resistance was reported by Amrollahi et. al. for GO and polyaniline-modified GO epoxy nanocomposites [34]. The importance of graphene-based additives has been established and explored with various modifiers, which enhance interfacial compatibility and dispersion of nanoparticles compared to unmodified ones.

The aim of the present study is to assess GO contribution into water absorption and hydrothermal ageing of an industrial epoxy adhesive. An efficient route was applied for GO functionalization by introducing amino groups onto the GO surface and mimicking in that way structure of the hardener, thus enabling the formation of chemical bonds with the epoxy and providing high interfacial adhesion, superior reinforcing efficiency and enhanced resistance to hydrothermal ageing. Anomalous water absorption behaviour accompanied with progressive weight losses is modelled by three different models considering additive or coupled contributions of water diffusion and leaching of epoxy components. The results of the study will contribute to the enhancement of global durability of common engineering adhesives and extension of their lifetime by introducing low amounts of efficiently modified GO nanoparticles.

2. Experimental details

2.1. Materials

The epoxy system used is an industrial system consisting of two main components: bisphenol-A-(epichlorohydrin) epoxy resin (component A) and amine-based curing agent (component B) sold under trademark Sikadur®-52, Sika Corporation, USA. The system is characterized as moisture-tolerant, high resistance epoxy resin with low viscosity (430 mPa s at 20 °C) and pot life of approximately 30 min. Epoxy adhesives contains several additives to control curing process and final properties. Component A consists of bisphenol-A-(epichlorhydrin) epoxy resin (50 – 100%), 1,3-bis(2,3-epoxypropoxy)-2,2-dimethylpropane (10 – 20%), [[(2-ethylhexyl) oxy]methyl] oxirane (2-ethylhexyl glycidyl ether) (10 – 20%), heavy aromatic solvent naphtha (petroleum) (2 – 5%), 2-methylnaphthalene (1 – 2%). Component B consists of Benzyl alcohol (20 – 25%), Aliphatic Amines (20 – 25%), Isophoronediamine (10 – 20%), Phenol 4-nonyl branched (10 – 20%), 2,4,6-tris(dimethylaminomethyl)phenol (5 – 10%), heavy aromatic solvent naphtha (petroleum) (5 – 10%), 2-methylnaphthalene (1 – 2%). The following chemicals were used in the GO synthesis; they were used as received or diluted to a specific concentration. Graphite flakes (99% carbon basis, -325 mesh particle size (≥99%), natural), sulphuric acid (95-97%), sodium nitrate (≥99.0%), potassium permanganate (≥99.0%), hydrogen peroxide (30%), hydrochloric acid (37%), methyl tert-butyl ether (≥98%), *N,N*-dimethylformamide (≥99.8%), acetic anhydride (≥99%) were purchased from Sigma-Aldrich.

2.2. Fabrication of experimental systems

2.2.1. Synthesis of GO

A modified Hummers method was applied to prepare GO from graphite [35,36]. Under continuous stirring in Erlenmeyer flask, 5.00 g graphite was mixed with 115 mL of concentrated sulphuric acid. Followed by the addition of 2.50 g sodium nitrate mixed with 15.00 g of potassium permanganate for 35 min, while the temperature was slowly controlled to remain under 37 °C. Stirring was continued for 2 h more followed by the addition of a half kilogram of ice. After the ice melted a small amount of hydrogen peroxide (25 wt.% solution) was added and sediment was filtered. Obtained GO was washed with diluted hydrochloric acid and water followed by centrifuging and drying in a vacuum. Rewashing was performed with methyl tert-butyl ether followed by the addition of water, which was separated by centrifuge, and GO was dried in a vacuum.

Details on structural characterization of the prepared GO by Fourier transform infrared spectroscopy (FTIR) and X-ray diffraction (XRD) are shown in Supplementary Material. FTIR spectra (Fig. S1) was used to characterize GO and signature peaks were identified at 3100-3400 cm^{-1} (O–H stretching), 1738 cm^{-1} (C=O stretching), 1611 cm^{-1} (C=C stretching), 1365 cm^{-1} (C-OH deformation), 1228 cm^{-1} (C–O–C stretching) and 1048 cm^{-1} (C–O stretching) [37]. Further assessment of GO structure was performed with X-ray powder diffraction (XRD) and spectra can be seen in Fig. S2. Bragg's equation was used to determine layer spacing (d) and obtained value d = 0.809 nm (2θ = 10.94º) confirmed GO structure, while no peak at 26.5° related to graphite structure was detected [38].

2.2.2. Synthesis of aldehyde functionalized GO

2 g of previously prepared GO was suspended in 16 mL of dimethylformamide and 3.6 mL of acetic acid anhydride was added with dropping funnel slowly over 30 min. The flask was heated in boiling water for 4 h and cooled afterwards at room temperature. pH was stabilized at around 4 with sodium acetate, followed by filtration and washing with acetone, diluted hydrochloric acid and methyl tert-butyl ether. The final product (GO-CHO) was dried under a vacuum.

The structure of GO-CHO was confirmed by FTIR spectra (Fig. S3): peaks at 3100-3400 cm^{-1} (O-H stretching), 2720-2830 cm^{-1} (C–H stretching aldehyde), 1771 cm^{-1} (C=O stretching aldehyde), 1705 cm^{-1} (C=O stretching), 1579 cm^{-1} (C=C stretching), 1374 cm^{-1} (C–OH deformation), 1232 cm^{-1} (C–O–C stretching) and 1053 cm^{-1} (C–O stretching) were identified [39]. XRD spectra (Fig. S4) indicated clear changes with two pronounced 2θ peaks at 11.84° and 42.34°, while layer spacing d = 0.748 nm (2θ = 11.84°) value decreased due to stronger interactions like the formation of hydrogen bonds.

2.2.3. Synthesis of amine-functionalized GO

1.5 g of GO-CHO was mixed with 1.5 g of ethylenediamine, 50 mL acetonitrile and few drops of concentrated acetic acid. The prepared suspension was left at 70 °C under continuous stirring for 24 h, then washed with acetone. The final amino group modified GO product (mGO) was dried under vacuum.

The structure of mGO was confirmed by FTIR spectra (Fig. S5): peaks at 1748 cm^{-1} and 1645 cm^{-1} (C=O stretching), 1520-1590 cm^{-1} peaks overlap (C=C stretching and N–H deformation), 1378 cm^{-1} (C–OH deformation), 1201 cm^{-1} (C–N and C–O–C stretching) and 1044 cm^{-1} (C–O stretching) were identified [37], [39]. XRD spectra (Fig. S6) shows layer spacing d = 0.384 nm (2θ = 23.14°) indicating stronger intermolecular interactions. 2θ peak was also observed at 42.7°, which remained relatively unchanged between the synthesis stages. Traces of GO-CHO were observed in the final products with XRD and FTIR. The GO formation procedure and the structure of the final mGO are shown in Fig. 1.

2.2.4. Composite preparation

The produced mGO was mixed into the amine-based hardener using ultrasonication. Then, epoxy was mixed with the hardener/mGO mixture using the ratio 2:1 by volume via ultrasonication. The concentration of added mGO was selected as 1, 2 and 5 wt. % of the hardener, thus the overall mGO concentration for the system was approximately 3 times lower. The compositions were cast in a Teflon mould and cured overnight at room temperature. Post-curing was performed for at least 12 h at 60 °C in an oven. Completeness of curing reaction was confirmed by absence of exothermic peaks on DSC diagrams of the samples (Supplementary material, Fig. S7). A neat epoxy and three epoxy/mGO systems were prepared, and their compositions are reported in Table 1. T_g of the neat epoxy cured under the specified conditions was 61 °C (Sec. 3.3.1). Volume contents of mGO were calculated by using ρ_{epoxy} = 1.15 g/cm^3 and $\rho_{graphite}$ = 2.2 g/cm^3 for mGO [40].

Table 1
The prepared epoxy/mGO composites.

Sample	mGO, wt.%	mGO, vol%	ρ^*, g/cm^3
epoxy	-	-	1.146 ± 0.0014
0.34 mGO	0.34	0.18	1.151 ± 0.0002
0.68 mGO	0.68	0.36	1.152 ± 0.0006
1.72 mGO	1.72	0.90	1.161 ± 0.0006

* determined experimentally by hydrostatic weighing in isopropanol.

Samples of average dimensions 2.5 × 5.2 × 40 mm^3 were cut from the casted plates and polished with sandpaper.

2.3. Methods

2.3.1. Water absorption

Two testing temperatures were selected for studying water absorption: T = 20 and 50 °C. The former corresponds to the glassy region, while the latter approaches the glass-to-rubbery state transition of the epoxy. Samples were immersed in distilled water using glass containers; one of them was kept under room temperature and the other one was placed in a thermostat with the fixed temperature. Weight changes of samples were periodically monitored with an accuracy of 0.01 mg. Before weighing, the surface of the samples was wiped using tissue paper. The relative weight change w [%] was determined by the following equation:

$$w = \frac{m_t - m_0}{m_0} \times 100, \quad (1)$$

where m_t is the weight of the wet sample at time t, and m_0 is the weight of the dry sample. Weight changes were measured using 6 replicates for each composition and test temperature with continuously decreasing intervals between measurements. The total duration of the tests was 12 months.

The density of samples was evaluated by hydrostatic weighing of samples in isopropanol (ρ = 0.786 g/cm^3). Measurements were done using 3 replicates of each composition in the reference state and after hydrothermal ageing. The density values for the reference samples are listed in Table 1.

2.3.2. Extraction in solvent

An amount of dissolved sol fraction was determined by common Soxhlet extraction procedure in acetone for at least 60 h. The samples before and after extraction were weighed with analytical balances. 3 parallel measurements were performed for each sample.

2.3.3. Dynamic mechanical thermal analysis

Dynamic mechanical thermal analysis (DMTA) was performed in a tension mode on a Mettler Toledo TMA/SDTA861e device equipped with a small tension clamp assembly. Tests were carried out on the reference (as-produced, dry) samples and after water absorption (aged for 7 months: denoted as w20 and w50 corresponding to the immersion temperature of 20 and 50 °C, respectively). Frequency 10 Hz, heating rate of 3 K/min, displacement amplitude of 5 μm, force amplitude 10 N, and a temperature range from 20 to 100 °C measurement parameters were used. These conditions were adjusted based on the data of strain sweep tests showing the linear viscoelastic response of the materials in the considered region. Reference samples were also tested under frequencies 0.1, 1, and 100 Hz to evaluate the activation energy. The basic tests with 10 Hz frequency were repeated for two reference replicates, while the rest tests were done for one representative

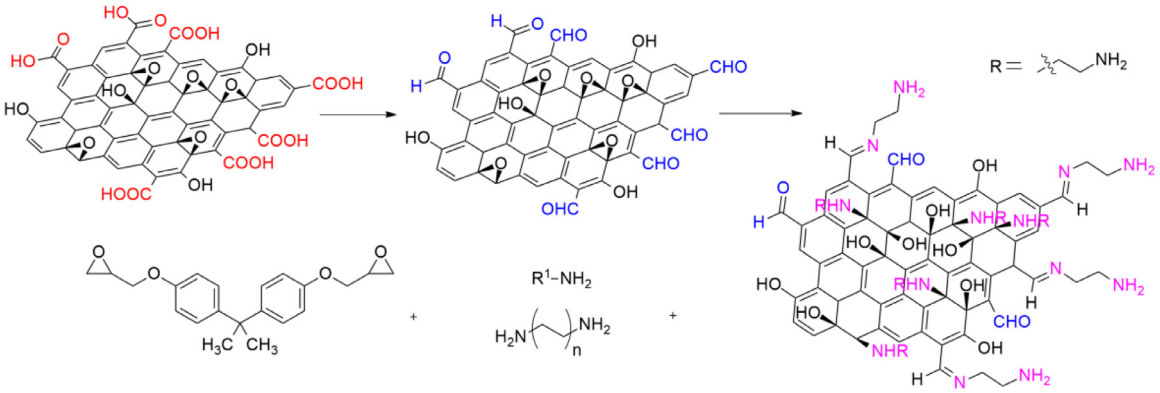

Fig. 1. GO modification scheme and formation of epoxy/mGO composition.

sample for each composition/ageing environment. In total, data of 30 DMTA tests are analysed.

2.3.4. Fourier transform infrared spectroscopy

Fourier transform infrared spectroscopy (FTIR) Nicolet 6700 (ThermoScientific, Germany) configured in attenuated total reflectance mode was used for composite investigation. Sixteen measurements were done in the region of 800 – 4000 cm^{-1} with a resolution of 4 cm^{-1}, and an error for the average spectrum was 1%. Spectra of the reference samples and aged in the water at 50 °C for 40 days were analysed. During this period weight changes of samples achieved an apparent equilibrium followed by weight losses (Sec. 3.1).

2.3.5. Scanning electron microscopy

Morphological characterization was performed by scanning electron microscopy (SEM) analysis of samples' surfaces that were prepared by a fracture in liquid nitrogen. TM3000 TableTop scanning electron microscope (Hitachi) was used with 5 to 15 kV voltage.

2.3.6. Optical analysis

Yellowing of samples was quantitatively estimated from photos of the reference, w20 and w50 samples after about six-months of conditioning. Photos were made in a "white box" and the luminosity factor (Adobe Photoshop) was determined for the measured area of 200 × 200 pixels by the intensity of RGB channels.

3. Results and discussions

3.1. Water absorption

Water absorption curves at T = 20 and 50 °C are shown in Fig. 2. Weight changes are plotted versus square root of time divided by the thickness of samples $\sqrt{t}/a$ to analyse the data within the framework of Fick's model and eliminate the influence of thickness variations from sample to sample [7]. As seen from the graphs, the test temperature is a determining factor affecting the overall character of water absorption. At room temperature and early time of weight change monitoring, samples possessed the Fickian-type diffusion behaviour: the curves show linear dependence at the start of water absorption, whereupon saturation is approached. Neat epoxy and nanocomposites showed similar behaviour, although the latter is characterized by lower diffusion rates indicated by the decreased slope of the curves. It can be noticed from Fig. 2a that some deviations from the Fickian diffusion appear after approaching equilibrium at $\sqrt{t}/a$ >15 (more than 2 months). Under elevated temperature, anomalous water absorption behaviour is observed: a very short linear part of the curves

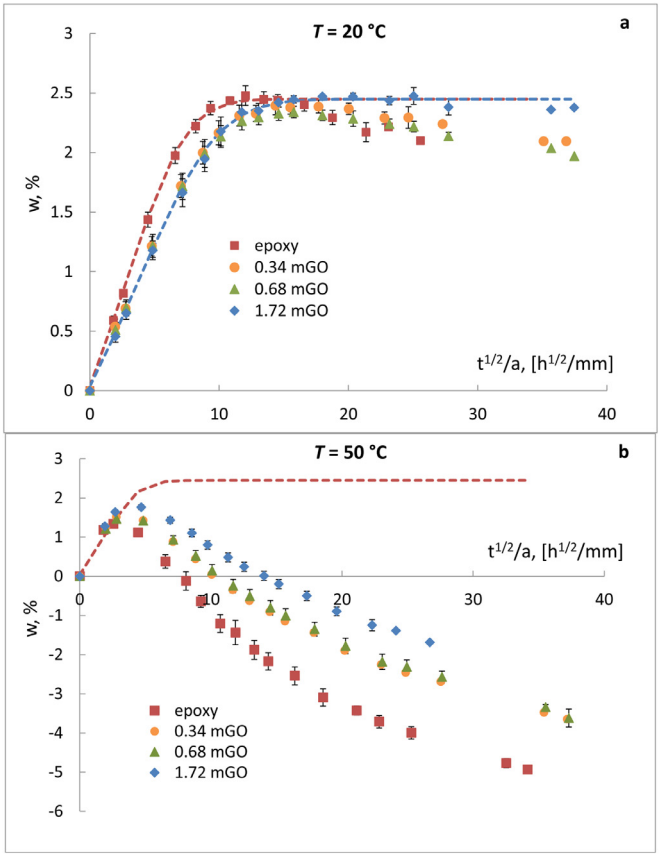

Fig. 2. Weight changes of samples during immersion in water at 20 °C (a) and 50 °C (b). Lines are approximations by Fick's model.

(for $\sqrt{t}/a$ < 3 corresponding to about 2 days) followed by dramatic weight decrease instead of equilibrium. Such a trend is observed for samples of both neat epoxy and filled with mGO. Nanocomposites possessed slightly delayed and lower weight losses compared to the neat epoxy with the lowest deviations from the Fickian behaviour for 1.72 mGO samples.

Weight losses of samples could be related to leaching of starting (e.g. petroleum, methylnaphthalene, benzyne alcohol etc. present in this industrial adhesive) and unreacted materials and/or low molecular weight species formed due to hydrolysis [10–15,20]. The former mechanism is obviously the predominant one for the present epoxy system considering its chemical structure and specific kinetics of leaching. According to extraction tests, 11.4 ± 0.29% and 8.7 ± 0.42% were leached from unaged neat

epoxy and 1.72 mGO samples, respectively. After conditioning of samples in hot water for about one year, these values decreased down to 5.9 ± 0.56% and 5.5 ± 0.46% and, thus, an amount of leached out into water species is estimated as 5.4% for neat epoxy and 3.2% for 1.72 mGO sample. These data correlate well with data presented in Fig. 2b.

Three different models were utilized to assess the kinetics of samples' weight changes. Model I and Model II consider additive contribution of two competitive processes taking place during water immersion tests: water diffusion into the sample and leaching of epoxy components from the sample into water. Then, the total weight change is given as a sum of the diffusion w_d and leaching w_l components

$$w^{I,II}(t) = w_d(t) + w_l^{I,II}(t) \quad (2)$$

The well-known Fick's equation was used for the description of the diffusion component [37,38]

$$w_d(t) = w_{d\infty}\left[1 - \frac{2}{\pi^2}\sum_{m=1}^{\infty}\frac{\left[1-(-1)^m\right]^2}{m^2} exp\left[-\left(\frac{\pi m}{a}\right)^2 Dt\right]\right] \quad (3)$$

where $w_{d\infty}$ is the equilibrium water content, D is the diffusion coefficient, and a is the thickness of the sample. The initial water content at $t = 0$ is assumed to be zero. 1D through-thickness diffusion is considered since the contribution from other directions is estimated as negligible.

Weight losses during samples' immersion in water are taken into account by two different ways (Model I and Model II). In Model I, the leaching mechanism is assumed to be a first-order kinetic process [43]

$$\frac{dw_l^I}{dt} = k\left(w_{L\infty} - w_l^I\right) \quad (4)$$

where $w_{L\infty}$ is the equilibrium (maximum) content of dissolved components for t → ∞ and k is the leaching rate constant. By assuming zero-content of dissolved components at $t = 0$, the solution of Eq. (4) is

$$w_l^I = w_{L\infty}\left(1 - e^{-kt}\right) \quad (5)$$

Model II assumes that leaching of soluble species from the polymer into water is driven by a similar to water diffusion mechanism and could be described by the mathematical expression similar to Eq. (3):

$$w_l^{II}(t) = w_{L\infty}\left[1 - \frac{2}{\pi^2}\sum_{m=1}^{\infty}\frac{\left[1-(-1)^m\right]^2}{m^2} exp\left[-\left(\frac{mk}{a}\right)^2 D_l t\right]\right] \quad (6)$$

where $w_{L\infty}$ is the equilibrium (maximum) content of dissolved components and D_l is the leaching rate constant. Similar considerations were applied in [20] for DGEBA epoxy-based glass fibre reinforced composites.

According to Model I and Model II, the total weight change of a sample when considering infinite time span (all processes reached equilibrium) is described by the relation

$$w_\infty(t \to \infty) = w_{d\infty} + w_{L\infty} \quad (7)$$

An alternative approach, presented by Model III, assumes coupled action of water diffusion and leaching of polymer molecules similarly to the diffusion-relaxation model [44]. The total weight changes are expressed as follows [15,44]:

$$w^{III}(t) = \left(1 + K\sqrt{t}\right) \cdot w_d(t) \quad (8)$$

where K is the leaching rate constant analogous to the relaxation related constant but taking negative values. As seen from Eq. (8), contribution of the leaching component into the total weight changes increases with time and the amount of absorbed water. Model III could be considered as a prototype of an autocatalytic process, when leaching is activated by the diffused water. It is worth noting that, different from Model I and Model II, this model doesn't assume saturation for the leaching-related component.

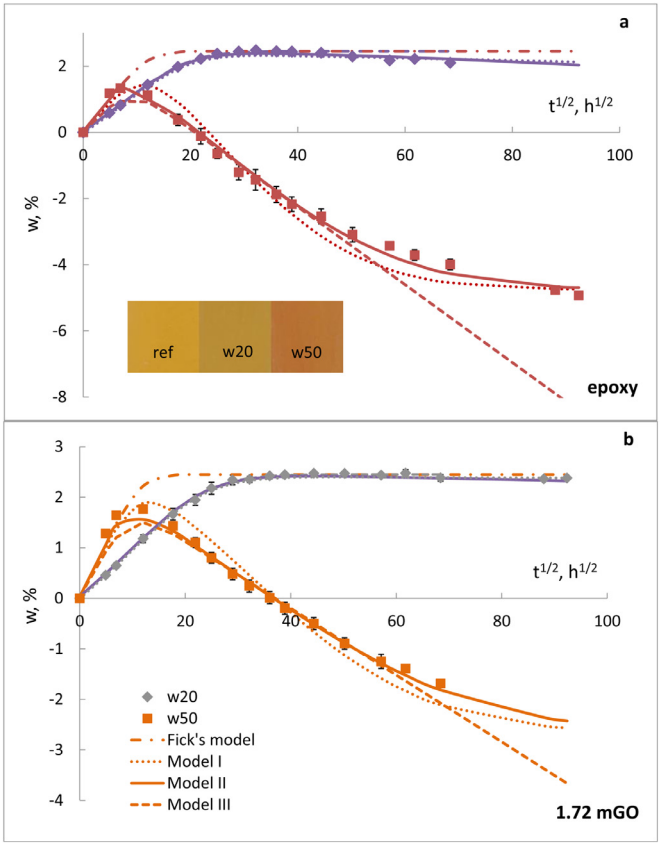

Fig. 3. Weight changes of w20 (diamonds) and w50 (squares) samples of the neat epoxy (a) and 1.72 mGO (b). Lines are calculations by Fick's model, Model I, Model II and Model III. Insert in (a) are photos of samples demonstrating their colour changes after 6-months exposure.

The results of the experimental data approximation are plotted in Fig. 3 for the neat epoxy and 1.72 mGO samples and Supplementary material, Figs. S8, S9. The fitting lines correspond to Fick's model obtained from Eq. (3), Model I by using Eqs. (2), (3), (5), Model II by using Eqs. (2), (3), (6), and Model III by using Eq. (8). The fitting parameters, obtained by calculating the minimum of the target function using the least-squares method, are given in Table 2.

It was assumed that equilibrium water content due to water diffusion $w_{d\infty}$ and equilibrium content of non-bound components $w_{L\infty}$ are temperature-independent parameters of the materials. As it is seen from Fig. 2b, samples exposed at elevated temperature didn't reach the "upper" limit, i.e. water diffusion equilibrium. To minimize uncertainties due to an arbitrary choice of fitting parameters, it was assumed that $w_{d\infty}(50\ °C) = w_{d\infty}(20\ °C)$. This assumption is in agreement with data of other researchers demonstrating negligible influence of temperature on the equilibrium water content in amine-cured epoxy resins of different chemical structure [45] and other epoxy systems [46]. In general, solubility and water saturation of epoxy could be affected by aging temperature, although these effects are more likely to be observed in not fully cured systems or epoxies with an excess of a hardener [47]. $w_{d\infty}$ is uniquely determined from the plateau in Fig. 2a. For de-

Table 2
Parameters of Fick's model, Model I, Model II and Model III.

Sample	$w_{d\infty}$% Fick's model	$D10^3$ mm^2 h^{-1}	$w_{L\infty}$% Model I, Model II	$k10^5$ h^{-1} Model I	D_l10^5 mm^2 h^{-1} Model II	$K10^3$ h$^{-1/2}$ Model III
T = 20 °C						
epoxy	2.45	3.5 ± 0.3	-7.2	0.7	0.035	-1.0
0.34 mGO	2.42	2.0 ± 0.2	-6.0	0.6	0.02	-0.7
0.68 mGO	2.35	2.0 ± 0.2	-6.0	0.6	0.02	-0.7
1.72 mGO	2.45	2.0 ± 0.2	-5.1	0.3	0.01	-0.3
T = 50 °C						
epoxy	2.45	10	-7.2	76	40	-48
0.34 mGO	2.42	10	-6.0	60	27	-37
0.68 mGO	2.35	10	-6.0	60	27	-37
1.72 mGO	2.45	10	-5.1	48	23	-27

termination of $w_{L\infty}$, on the contrary, weight changes at 50 °C are considered as the determining ones. As seen from Fig. 2b, an apparent "lower" equilibrium is approached for all samples within one year of weight change monitoring. Then, by taking into account Eq. (7) $w_{L\infty}$ is equal to w_∞ (experimental data) minus $w_{d\infty}$ uniquely determined at 20 °C. Thus, each of the models has only one fitting parameter accounting for weight loss, i.e. the leaching rate constant k, D_l and K for Model I, Model II and Model III, respectively. As seen from the data of Table 2, the leaching constants significantly (for more than three orders) increased with elevated temperature. Interestingly, water diffusion coefficients follow less extensive dependence on temperature and their values increase only by a factor of five or less when comparing the data for 20 and 50 °C. According to data for Model I and Model II, water diffusion into the samples occurs at a much higher rate than leaching of dissolved species from samples into the water: e.g. D and k values differ for more than 10 and 100 times at 20 °C and 50 °C, respectively. In the coupled diffusion-leaching model, K have comparable to D values. An amount of leached species is very high (7.2% for the neat epoxy) raising environmental concerns for using such epoxy systems in water-based environments [23].

As seen from the data of Figs. 2, 3 and Table 2, incorporation of mGO into the epoxy resulted in the minor decrease of the equilibrium water content $w_{d\infty}$ (changes within 0.1%), while the diffusion coefficient at 20 °C decreased for more than 40%. However, this difference in D values for samples with different contents of mGO disappears at 50 °C. Equilibrium content of dissolved epoxy components $w_{L\infty}$ greatly decreased with the addition of the nanofillers (by comparing the absolute values): the highest decrease is obtained for 1.72 mGO samples, for which $w_{L\infty}$ is for 2.1% lower than that one of the neat epoxy. This difference correlates well with data of extraction tests (2.7% by comparing neat and mGO-filled unaged samples). The leaching rate constants k, D_l and K also greatly decrease with a higher content of mGO in epoxy: down to 70 and 40% at 20 and 50 °C, respectively. Obviously, mGO i) act as barriers for both water diffusion inside and leaching outside and ii) retard relaxation processes in epoxy by hampering movements of polymer chain segments and subsequent extraction of low molecular weight components. Addition of mGO could also affect curing kinetics of epoxy [65] and result into lower amount of unreacted materials, however these issues need further investigations. Differences in the leaching rates between the neat epoxy and nanocomposites greatly diminish at 50 °C that is related to the competitive nature of two factors: segmental mobility of a polymer and tortuosity of the diffusion path caused by the presence of the nanosized inclusions. At elevated temperatures, the contribution from the tortuosity is diminished by an increase in segmental mobility of the polymer, water and dissolved molecules [7,42].

All three models demonstrate rather good approximation results at 20 °C, while noticeable differences between their effectiveness are observed at elevated temperature (Fig. 3, Supplementary material Figs. S8, S9). Model II shows the best fit to the experimental data within the entire time range, while Model I could give reasonable data fitting in a specific time span only. Model III is effective up to $t^{1/2}$= 50 – 60 h$^{1/2}$, although this results in too rapid and overestimated weight losses at longer times. Despite known limitations of the models, their main advantages are physical origin, tractability, and involvement of only one additional fitting parameter (leaching rate).

Similar observations on weight loss during water immersion tests have been reported for unsaturated polyester [17], vinylester [15] and DGEBA/DDA epoxy [12]. Authors indicated to negligible weight losses at room temperature, while anomalous behaviour was observed at elevated temperatures approaching T_g of polymers. The plasticization of the polymer network due to high temperature and water diffusion facilitated higher extraction of soluble species, thus producing a more rigid matrix, which appeared as an increased T_g value of water-aged samples. Hydrolysis effects in an epoxy-anhydride system due to water ageing are proposed by Capiel et.al. [13], although anomalous water absorption behaviour resulted in a dramatic weight increase of samples. Additional water ingress into samples was facilitated by hydrolytic scissions of the epoxy confirmed by FTIR and pH variations. Similar considerations on hydrolysis-driven water absorption supplemented by the diffusion-reaction model are described by Yagoubi et.al. for another anhydride-cured epoxy [14] and non-stoichiometric amine-cured epoxies [11]. In epoxy-based fibre reinforced composites, weight losses of samples during their exposure to water is commonly explained by hydrolytic degradation of the fibre-matrix interphase [20,22]. Anomalous water diffusion in epoxy/carbon nanoparticles composites has been studied in [7,22,40]. A continuous increase of weight changes of samples after approaching the apparent "Fickian" equilibrium was lower for nanocomposites. This fact was explained by lower contribution from the relaxation-driven water diffusion mechanism and quantitatively characterized by the reduced relaxation times in the nanoparticle-reinforced epoxy [7]. Alternatively, a nondimensional hindrance coefficient is introduced in the Langmuir-type model used for the description of non-Fickian two-stage water diffusion in carbon/epoxy nanocomposites [48]. The molecular bonding during diffusion, as well as the interfacial moisture storage, are also mentioned among the reasons for non-Fickian behaviour. A thermo-diffuso-mechanical model based on a thermodynamic framework was proposed by Leger et.al. to describe non-classical water diffusion of an industrial rubber toughened epoxy adhesive [21]. In the latter model, the increased water uptake was taken into account by the increased cavitation of a swollen material. Neither experimental or theoretical studies on weight losses in epoxy matrixes were found in literature.

Structural changes and degradation of properties are often indicated by simple observations like changes in colour. Noticeable colour changes were observed for the water-aged epoxy under study. Photos of epoxy samples after conditioning in air and wa-

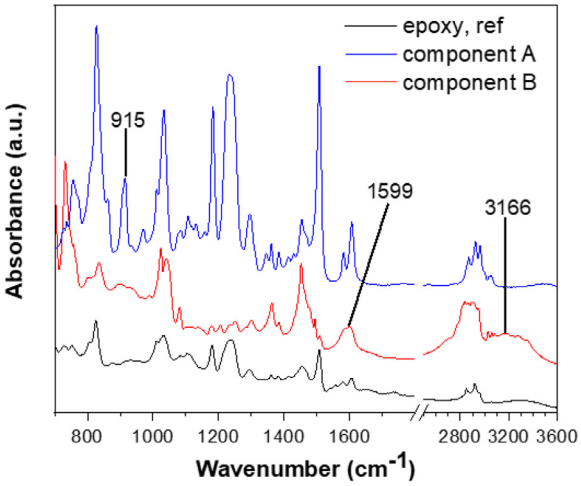

Fig. 4. FTIR spectra of the cured epoxy system and its components.

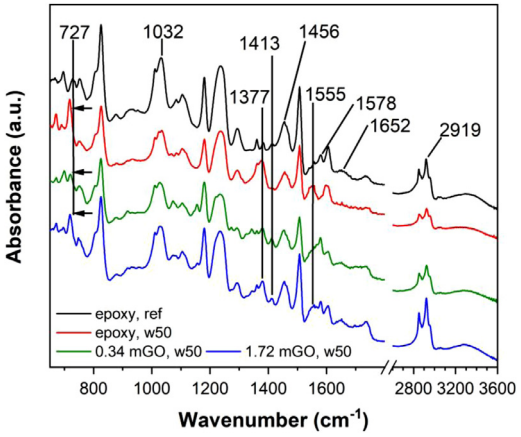

Fig. 5. Absorbance peaks of FTIR spectra for water-aged samples.

Table 3
DMTA characteristics at 10 Hz of the reference and water-aged samples.

Sample	T_g,°C	E'_g, GPa 25 °C	E'_r, MPa 100 °C	tan δ
reference				
epoxy	60.9 ± 0.6	1.42 ± 0.04	9.48 ± 0.39	0.60 ± 0.00
0.34 mGO	67.9 ± 1.6	1.87 ± 0.24	12.50 ± 2.34	0.54 ± 0.02
0.68 mGO	66.9 ± 1.0	2.08 ± 0.05	13.66 ± 0.48	0.64 ± 0.06
1.72 mGO	70.0 ± 1.8	2.31 ± 0.01	15.99 ± 0.69	0.65 ± 0.01
w20				
epoxy	43.4	0.55	8.5	0.45
0.34 mGO	51.6	1.03	13.5	0.47
0.68 mGO	52.0	1.09	13.7	0.46
1.72 mGO	58.5	1.36	16.5	0.48
w50				
epoxy	61.9	1.61	11.4	0.62
0.34 mGO	62.2	1.69	13.7	0.59
0.68 mGO	62.3	1.68	13.8	0.56
1.72 mGO	63.9	1.84	16.1	0.57

ter for the same time (about six months) are shown in the insert of Fig. 3a. The yellowing and reduced transparency of the aged epoxy progressed more in elevated temperature. The yellow starting colour of samples transforms into a progressively darkened orange. The luminosity factor was estimated as 7%, 9%, and 12% for the reference, w20 and w50 samples, respectively. Uniform colour changes occurred in the cross-section of samples affirming yellowing as a bulk phenomenon rather than a surface only process. Similar observations were done for different epoxy systems linking the yellowing phenomena with hydrolytic reactions, oxidative evolution of carbonyl groups in the resin and extraction of monomers or oligomers [9,18,41]. Yellowing of the studied epoxy is related to the development of carbonyl groups as it was confirmed by FTIR observations (Sec. 3.2). It was observed that the density of w50 samples increased by approximately 0.5% compared to the reference samples (Table 1). This change could be explained by the formation of a more rigid polymer network facilitated leaching of the plasticizers and solvents from the polymer. These proposed explanations are further confirmed by FTIR and DMTA investigations.

3.2. FTIR analysis

Chemical structure analysis was performed with FTIR. Fig. 4 shows FTIR spectra of the cured epoxy system in comparison with component A (contains oxirane rings) and component B (contains primary amine groups). This graph is used to identify the conversion of oligomers into polymers, although similar commercial systems have been reported before. The signals at 1599 and 3166 cm^{-1} are signature peaks for NH_2 stretching and deformations, respectively [49,50], while the peak at 915 cm^{-1} is responsible for C–O stretching in the oxirane group [51]. It has also been reported that the presence of a very small amount of water can result in the broadening of the NH_2 stretching peak as can be observed [50]. None of these peaks is present in the prepared sample spectra indicating a complete epoxy curing reaction. Similar spectra have been obtained for all mGO/epoxy samples.

FTIR spectra for water-aged samples after conditioning at 50 °C for 40 days were compared to these for the neat epoxy. The neat epoxy was chosen as a representative reference sample since FTIR spectra of unaged epoxy and epoxy/mGO were almost identical. Samples 0.34 mGO and 0.68 mGO showed very similar results, thus only 0.34 mGO sample is used within FTIR discussion. Significant differences can be observed between the aged samples (Fig. 5). Changes in the peak intensities and positions are the greatest for the neat epoxy, while spectra of epoxy/mGO samples are less affected by hydrothermal ageing. The peak at 1032 cm^{-1} is the signature peak for symmetrical stretching vibrations C-O-C of ether structure (Fig. 5) [52,53]. The water-aged neat resin shows similar values to 0.34 mGO, although with a notable change in the peak shape. Another characteristic peak is C–O–C asymmetric stretching (Fig. 5), which has a rather broad peak due to various amines used in industrial epoxy resin products [50,53]. The decreased peak intensities at 1032 and 1235 cm^{-1} are observed for all nanocomposites samples. The peak at 1456 cm^{-1} represents deformation vibrations of C–H, CH_2 and CH_3 [49,52]. As it can be seen from Fig. 5, there are almost no changes for the nanocomposites samples indicating its high resistance to hydrothermal ageing compared to the neat epoxy sample, which showed not only decreased intensity but also shifted peak.

3.3. Dynamic mechanical properties

3.3.1. Reinforcement efficiency

Temperature dependences of the storage moduli $E\prime$ and loss factor tan δ for representative reference samples with various contents of mGO are shown in Fig. 6a. The basic DMTA characteristics: the glassy E'_g (25 °C) and rubbery E'_r (100 °C) storage moduli, T_g determined by tan δ peaks are listed in Table 3. Incorporation of mGO into the epoxy resulted in a noticeable increase of $E\prime$, in both the glassy and rubbery states. T_g of nanocomposites shifted towards higher temperatures compared to the neat epoxy. The greatest improvement in properties is obtained for 1.72 mGO composition: both E'_g and E'_r increase for more than 60%, while T_g is shifted for 10 °C. Samples with lower amounts of mGO showed

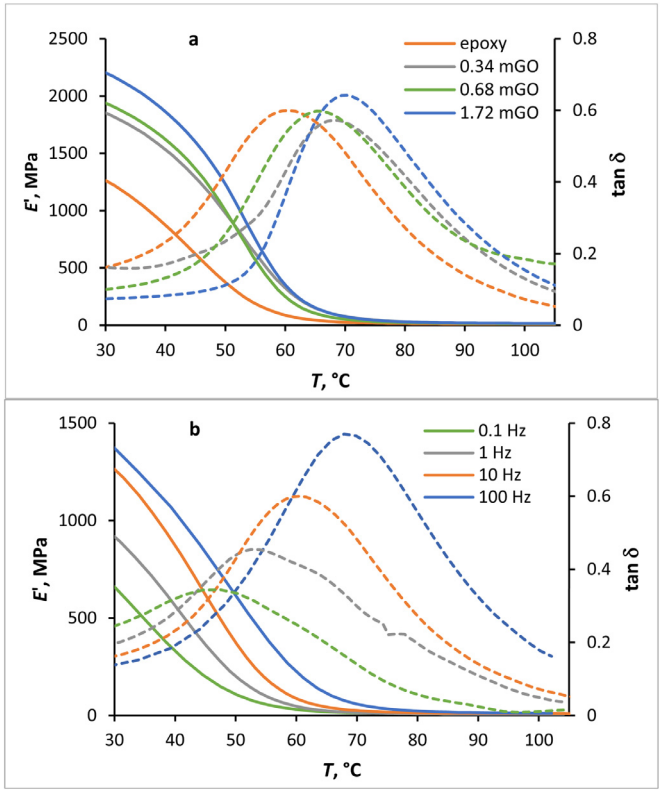

Fig. 6. Storage moduli (solid) and loss tangent (dashed lines) of samples in the reference state at 10 Hz (a) and different frequencies for the neat epoxy (b).

similar, albeit less pronounced, improvements of $E\prime$ and T_g. Damping properties (height and broadness of tan δ peak) of the epoxy were not significantly affected by the presence of mGO. The shape of Cole-Cole plots (loss modulus versus storage modulus in logarithmic axes shown in Fig. S10) looked like semicircle diagrams indicating structural homogeneity and good adhesion between the nanofillers and epoxy [54–56].

Nanofillers embedded into the polymer matrix provide a reinforcing effect and restrict motions of polymer chain segments that appear in higher E'_g and T_g of epoxy/mGO samples compared to the neat counterpart [6,7,24,25,42]. In nanocomposites, the increased E'_g is directly correlated to the degree of entanglement and dispersion efficiency, while increased E'_r is correlated with a higher degree of crosslinking and the degree of interaction between the polymer and the fillers [54,57]. The general effectiveness of the filler on the storage modulus of composites can be represented by the parameter C given by relation [54,55]

$$C = \frac{\left(E'_g/E'_r\right)_{composite}}{\left(E'_g/E'_r\right)_{matrix}} \quad (9)$$

For well-dispersed fillers and good compatibility with the polymer matrix, $C < 1$. The lower is C, the most efficient the reinforcement effect is. C factors of the nanocomposites under study are in the range of $0.8 < C < 1$ (Fig. 7). Despite data scatter, a common decreasing trend for C with growing content of mGO is obtained indicating a reasonable efficiency of the nanofiller.

The reinforcement efficiency factor r is an alternative and complementary parameter for the characterization of filler-matrix interactions and the overall effectiveness of reinforcement in a composite. Following simple Einstein's considerations for suspensions with rigid particles, the moduli of the composite E_c and the matrix

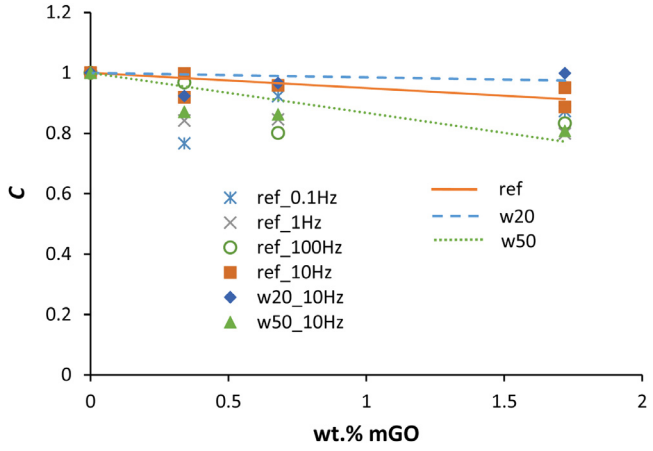

Fig. 7. C factor as a function of the weight content of mGO for reference samples tested at different frequencies and hydrothermally-aged samples tested at 10 Hz.

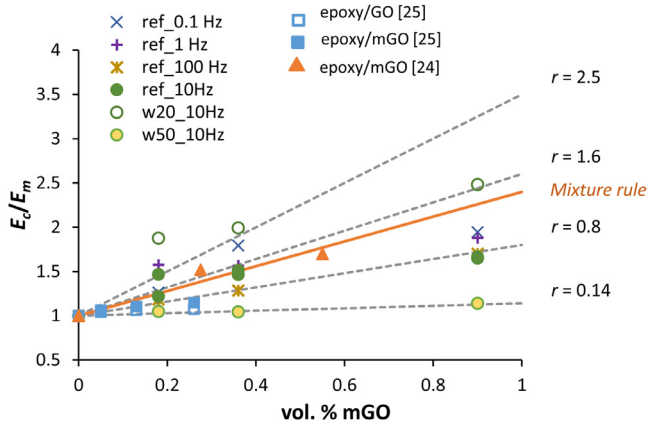

Fig. 8. The ratio of the glassy storage moduli according to Eq. (10) as a function of volume content of mGO for reference samples tested at different frequencies and hydrothermally-aged samples tested at 10 Hz.

E_m are related by an empirical relationship [54,57]

$$E_c = E_m\left(1 + rV_f\right) \quad (10)$$

where V_f is the volume fraction of filler in the composite. In the case of an incompressible matrix, perfect adhesion between the filler and matrix as well as perfect dispersion of individual filler particles, $r = 2.5$. For imperfect bonding and slippage in the interface $r < 2.5$. According to Eq. (10), plotting the ratio E_c/E_m versus V_f the slope gives r. Within the present study, the ratio of the glassy storage moduli is considered. E_c/E_m of the reference, epoxy/mGO samples are shown in Fig. 8 by filled circles. Dotted lines are linear trends with different r and the solid line is a calculation by the mixture rule with $E_f = 200$ GPa and $E_m = 1.42$ GPa (Table 3). As expected, E_f is highly underestimated compared to the elastic modulus of pure graphene (1 TPa), although this value agrees well with that one for the chemically reduced monolayer graphene oxide reported as around 0.25 TPa [58]. Poor dispersion, imperfect bonding between the filler and matrix, functionalization-induced defects, stacking of few layers instead of a single sheet, wrinkling etc. are some examples of factors affecting the effective modulus of graphene in composites [28,29,58]. For the reference samples, r values are in the range of 0.8 – 1.6. Similar reinforcing efficiency with $r \sim 0.7$ was reported for polycarbonate/graphene oxide composites (triangles in Fig. 8) [28]. Much lower improvements in the elastic modulus of about 10% and $r \sim 0.15$ were reported in [29] for epoxy reinforced with pristine and silane-functionalized graphene oxide (squares in Fig. 8).

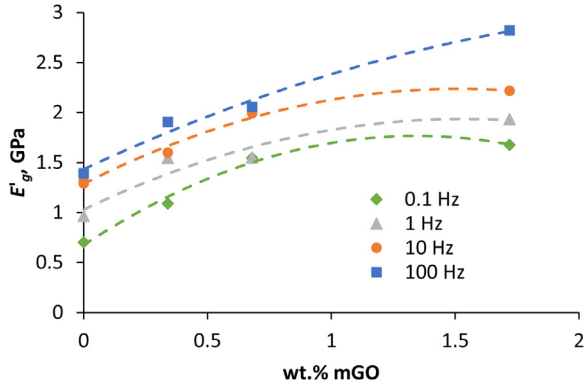

Fig. 9. Glassy storage modulus (25 °C) of the reference samples as a function mGO content at different frequencies.

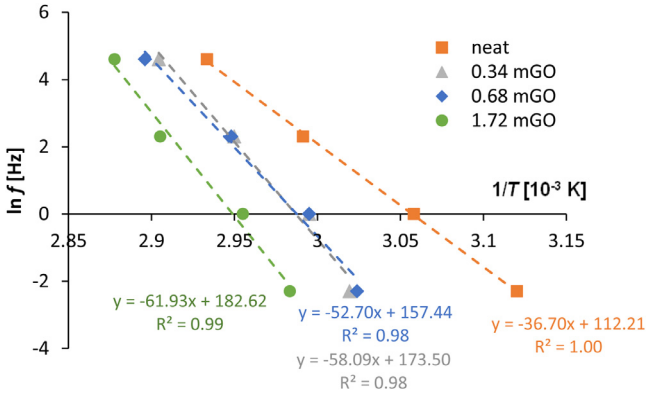

Fig. 10. ln(f) versus $1/T_g$ for the reference samples of epoxy/mGO.

As seen from Figs. 7 and 8 the reinforcement efficiency is highly influenced by test conditions (frequency and ageing state) and the method or parameter used. This fact introduces some uncertainties in data interpretation [57], however, could also be used for quantitative monitoring of the reinforcement efficiency under different conditions.

3.3.2. Frequency-dependent behaviour

The viscoelastic nature of polymers appears in their frequency-dependent thermomechanical properties. $E\prime$ and tan δ for the neat epoxy samples is demonstrated in Fig. 6b. Similar dependencies were also observed for epoxy/mGO samples. For all samples, $E\prime$ and tan δ is shifted to higher temperatures with increasing frequency. Such a behaviour is typical for many polymers and is explained by the decreased mobility of the polymer network at high frequencies since polymer chains do not have enough time for rearrangements [59–62]. At a low frequency, there are observed extremely broad loss peaks indicating a wide range of relaxation processes appeared in the polymer network structure. This could be explained by the involvement of large-chain segments in overall macromolecular motion and increased internal friction compared to that one in fast or high-frequency process, where the main contribution comes from small-chain segments [63].

E'_g of the reference epoxy/mGO samples at different frequencies are shown in Fig. 9. Qualitatively similar dependences were also observed for E'_r. For all test frequencies, E'_g and E'_r increase with growing content of mGO in epoxy confirming reasonably good reinforcing efficiency of the nanofiller. This fact correlates well with the frequency dependences of the parameters C and r in Figs. 7 and 8, respectively. An increase in absolute E'_g values with increasing frequency are almost the same for all compositions. This could be related to small differences in segmental motions of the polymer network in the neat epoxy and nanocomposites in the considered range of test time and temperature. However, this fact needs further investigations at higher temperatures and longer times (lower frequencies), when the contribution from hampered movements of polymer macromolecular chains and retarded relaxation processes in nanocomposites is expected [6,25]. Overall, within the same experimental time (frequency) span nanocomposites are characterized by higher dynamic moduli and thus, altered viscoelastic deformations compared to the neat epoxy.

The glass transition temperature T_g follows a typical Arrhenius relationship with frequency f that is widely used in the dynamic mechanical analysis [19,59–63]:

$$f = A \cdot exp\left[-\frac{\Delta E}{R \cdot T_g}\right] \text{ or } \ln(f) = \ln(A) - \frac{\Delta E}{R}\frac{1}{T_g}, \quad (11)$$

where ΔE is the Arrhenius activation energy for the glass transition relaxation, R is the ideal gas constant and A is a material constant. The relationships ln(f) versus $1/T_g$ for the reference samples are shown in Fig. 10. The data demonstrate reasonable approximations by linear trends with R-squared values in the range of 0.98−1.00. ΔE calculated from the slopes of the lines are 305, 482, 438 and 515 kJ/mol for the neat epoxy, 0.34 mGO, 0.68 mGO and 1.72 mGO samples, respectively. Great, almost twofold, increase of ΔE with growing mGO content indicates an increase of the energy barrier that must overcome the occurrence of molecular motions causing the glass transition in nanocomposites [56]. The increased ΔE is also an indicator of good adhesion between the filler and matrix [55]. It should also be noted that while T_g represents a relationship between the mobility of polymer chains and temperature, ΔE represents a relationship between mobility and time scale. This fact is used for the determination of the temperature shift factors and predictions of long-term properties by using time-temperature superposition principles [56,61,63]. The activation energy is directly related to the lifetime of materials: the higher ΔE, the longer the lifetime [64].

Similar considerations on the activation energies of epoxy/graphene nanocomposites were analysed in [65], where ΔE = 670 kJ/mol was found to be independent on the nanofiller loadings of 1 and 5 wt.%. In the study of Montazeri et.al. [56], ΔE of epoxy increased by about 10% with the addition of 0.5 wt.% of multiwall carbon nanotubes (from 455 to 510 kJ/mol), while the absolute values were dependent on curing conditions of the systems. In other studies, the activation energy of 277 kJ/mol and 345 kJ/mol were found for amine-cured epoxy [19] and vinyl ester resin [61], respectively.

3.3.3. Hydrothermal ageing effects

Temperature dependences of $E\prime$ and tan δ for the reference, w20 and w50 samples of the neat epoxy and 1.72 mGO are shown in Fig. 11. Similar curves were also obtained for 0.34 mGO and 0.68 mGO compositions. E'_g and T_g of the reference, w20 and w50 samples are compared in Fig. 12. Hydrothermal ageing greatly affected the dynamic mechanical response of the samples appeared in a dramatic drop of E'_g and shift of tan δ peaks to lower temperatures. The absolute values for DMTA characteristics are given in Table 3. The greatest influence is observed for the neat epoxy w20 samples: E'_g drops for more than 60% and T_g shifts for 18 °C compared to the reference samples. A decreasing trend in water-induced plasticization effects is observed with the growing content of mGO in epoxy. For 1.72 mGO samples, E'_g decreases for 40%, while T_g shifts for 11 °C only. The observed difference in plasticization effects of epoxy and nanocomposites is not related to the amount of absorbed water, since equilibrium water contents of

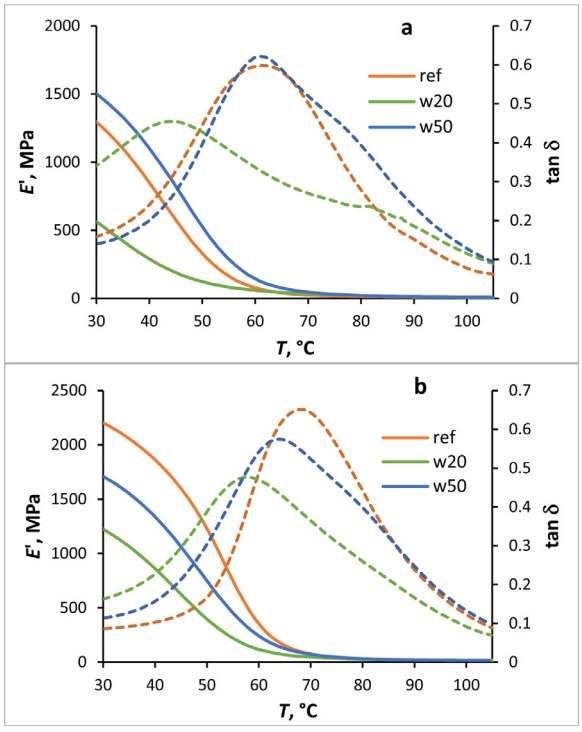

Fig. 11. Storage moduli (solid lines) and loss tangent (dotted lines) for the reference, w20 and w50 samples of neat epoxy (a) and 1.72 mGO (b) samples at 10 Hz.

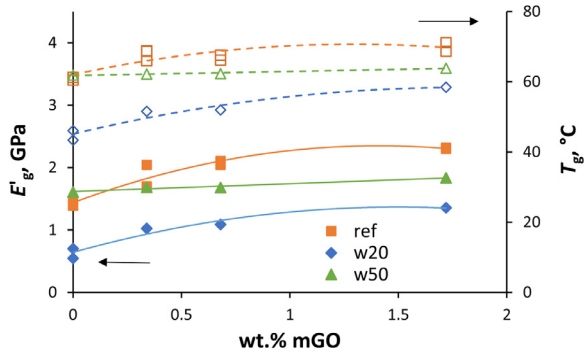

Fig. 12. Glassy storage modulus (filled symbols) and glass transition temperature (unfilled symbols) of the reference, w20 and w50 samples at 10 Hz. Lines are approximations.

all compositions were practically the same (Fig. 2, Table 2). Obviously, nanoparticles act as barriers for segmental motions of the plasticized polymer altering in that way the overall viscoelastic response. The decrease of T_g for the neat epoxy and 1.72 mGO sample is 7 and 4 °C per 1% of the absorbed water, respectively. These data agree well with literature data for similar epoxy systems [7,42] and epoxy/graphene composites [6]. The plasticization effect of absorbed water appears also in broadening and lowering of tan δ peaks, although to the same extent for both neat epoxy and nanocomposites. No significant differences between E'_r of the reference and w20 samples are noticed (Table 2). These facts indicate a reasonable crosslinking degree and interfacial adhesion between the epoxy and mGO maintained after long-term water absorption.

Unexpectedly, hydrothermal ageing at 50 °C possessed a much lower influence on thermomechanical characteristics of the samples than that at 20 °C. For nanocomposites, E'_g the decrease is within 20%, while T_g changes do not exceed 6 °C. Moreover, a slight improvement in E'_g and T_g is noticed for the neat epoxy. Such behaviour can be explained by a counterbalancing contribution from water-induced plasticization and additional crosslinking due to thermo-oxidation [9] or physical ageing effects [7,16,18]. Also, noticeable extraction of soluble nonreactive epoxy species resulted in the formation of a more rigid matrix [17] confirmed also by the increased density of w50 samples. Interestingly to note that hydrothermal ageing greatly diminished the positive effect from mGO: E'_g and T_g of w50 samples increases with growing mGO content to a much lower extent compared to the reference and w20 samples (Fig. 12). The decreased reinforcing efficiency is seen in Fig. 8 with r drop down to 0.14. Small differences between tan δ and E'_r values for the reference and w50 samples (Table 3) indicate a moderate influence of hydrothermal ageing on interfacial interactions between the epoxy and mGO. Fairly high E'_r values of w50 samples appeared in low C factors (Fig. 7) giving a contradictory result on the improved reinforcement efficiency of hydrothermally aged samples. Relatively good epoxy-mGO interfacial adhesion is further confirmed by SEM investigations.

3.4. Morphological characterization

Fracture surfaces of the reference, w20 and w50 samples of the neat epoxy and 1.72 mGO samples are shown in Fig. 13. The neat epoxy (Fig. 13 a, c, e) shows a flat surface with river-like patterns in the direction of fracturing force, while the nanocomposite has a rough and faceted surface (Fig. 13 b, d, f). Samples didn't exhibit large agglomerates, voids or defects indicating a reasonable dispersion quality of mGO in epoxy. Addition of amine groups on GO prevented agglomeration and promoted interactions between mGO and epoxy through the crosslinking process. A rough fracture surface of 1.72 mGO with many small facets on it indicates strong interfacial adhesion between mGO and epoxy since the nanoplatelets extend the fracture route [26,30,31].

Fracture surfaces of the hydrothermally aged epoxy samples are characterized by widened river-patterns related to the plasticization effect of water (Fig. 13 c, e). The surface of w50 samples is very smooth, typical for tough fracture, indicating a high contribution of plastic deformations due to plasticization effects. No apparent voids and cavities are observed for the water-aged epoxy samples, thus confirming the uniform and “molecular-scale” origin of the leaching process. Fractographs of 1.72 mGO aged samples show smoother surfaces with fewer contrast facets compared to the reference sample. In addition to the water-induced plasticization effect on epoxy, this fact is also attributed to the decreased interfacial adhesion between the filler and host polymer. Water ageing and weakened adhesion between mGO and epoxy resulted in the formation of small microchannels (indicated by arrows in Fig. 13 d, f) for w20 and w50 samples, although these are not many and are rather small. The results agree well with the high reinforcing efficiency of mGO on the epoxy that is maintained after hydrothermal ageing of samples.

4. Conclusions

An efficient three-step route was applied for GO production from graphite and GO functionalization. Amino groups were integrated into GO structure mimicking in that way structure of the hardener, thus enabling the formation of chemical bonds with the epoxy and providing high interfacial adhesion.

Water absorption by the amine-cured epoxy adhesive reinforced with functionalized GO was studied at 20 and 50 °C. Anomalous behaviour that appeared in the weight loss of samples was more extensive at elevated temperature and exceeded 7%. Nanocomposites are characterized by significantly lower water diffusivity (down to 40 % at 20 °C) and for about 2.1% decreased weight loss compared to the neat epoxy. Leaching of nonreacted epoxy compo-

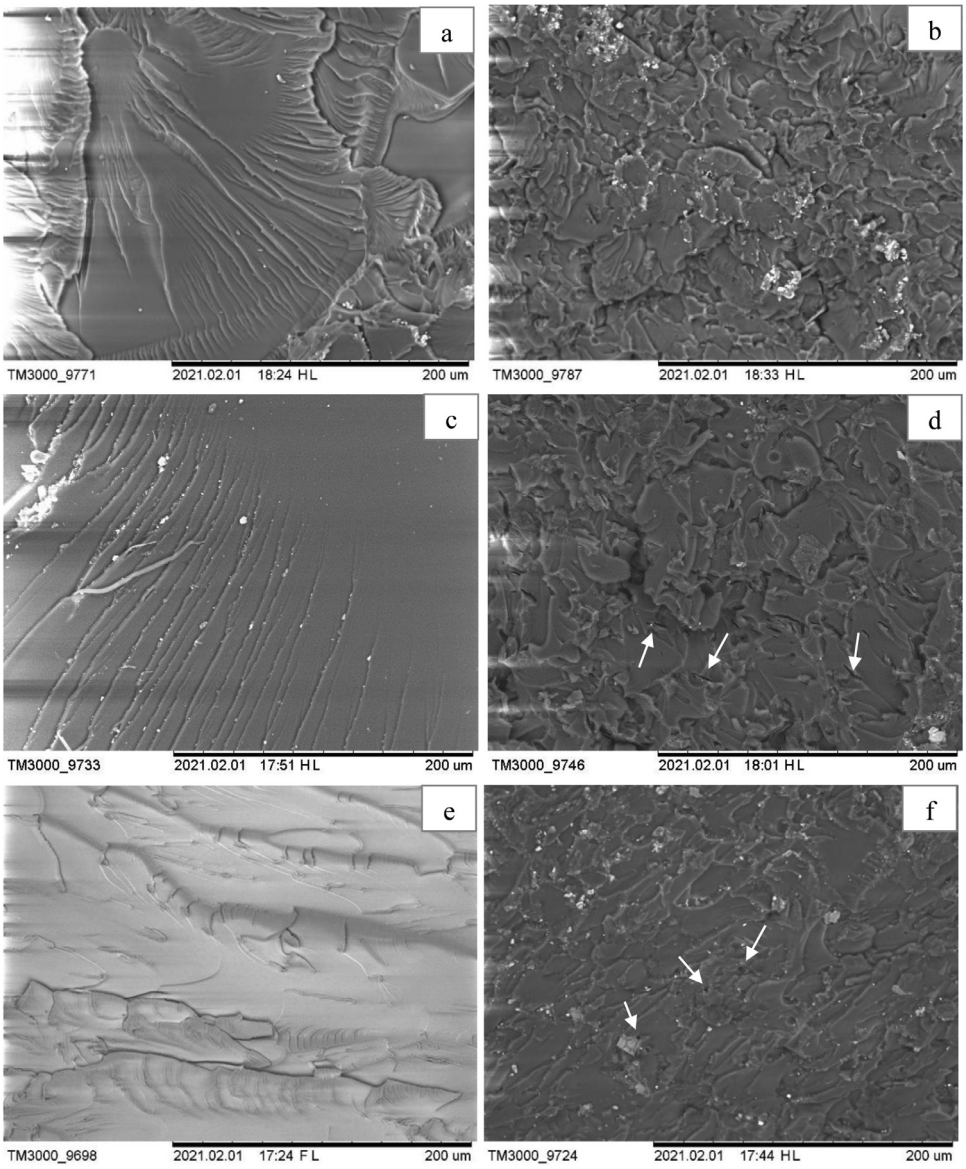

Fig. 13. SEM micrographs of neat epoxy (a, c, e) and 1.72 mGO (b, d, f) samples: reference (a, b), w20 (c, d) and w50 (e, f).

nents, as supported by solvent extraction tests, is the main mechanism contributing to non-Fickian diffusion. Three models considering additive or coupled contribution of water diffusion and leaching were applied for approximation of the experimental data. The leaching rate, the only additional fitting parameter introduced into all models, greatly decreased with the growing content of mGO down to 70%. Well dispersed mGO act as efficient barriers for both water diffusion inside and leaching outside and retard relaxation processes in epoxy by hampering movements of polymer chain segments and subsequent extraction of low molecular weight species. However, the contribution from the tortuosity effect is diminished at elevated temperature due to increased segmental mobility of the polymer, water and dissolved molecules.

FTIR analysis for epoxy/mGO samples revealed lower changes in shape and intensities of some characteristic bands compared to the neat counterpart explaining enhanced hydrothermal ageing resistance of nanocomposites.

Reasonably high reinforcement efficiency is obtained for epoxy/mGO compositions. Maximally loaded 1.72 mGO samples are characterized by the increased E'_g and E'_r up to 60%, higher T_g for 10 °C and an almost twofold increase of the activation energy of glass transition compared to the neat epoxy. Hydrothermal ageing resulted in noticeable properties degradation of samples caused by polymer plasticization and loss of epoxy-mGO interfacial adhesion. E'_g of the neat epoxy decreased by 60% and T_g decreased for 18 °C, while nanocomposites possessed high resistance to hydrothermal ageing. Under elevated temperature, properties degradation is partly counterbalanced by the formation of a more rigid polymer network facilitated by leaching of low weight species. The latter appears in the increased density and higher E'_g and T_g of w50 samples compared to w20 samples.

Smoothed fracture surfaces of water-aged samples studied by SEM confirmed the appearance of water plasticizing effect and loss of interfacial adhesion between the epoxy and mGO. Minor defects in the form of agglomerates and voids were observed on the surfaces indicating the high dispersion quality, filler-matrix compatibility and high resistance to hydrothermal ageing.

The results of the study will contribute to the enhancement of global durability of common epoxy adhesives and extension of their lifetime as well as decreasing environmental pollution from leaching of toxic epoxy components. The latter is extremely important for applications in water-based environments, e.g. marine in-

dustry. Quantitative assessment of the service lifetime of the neat epoxy and nanocomposites will be presented in the next study.

Declaration of Competing Interest

The authors declare that they have no known competing financial interests or personal relationships that could have appeared to influence the work reported in this paper.

CRediT authorship contribution statement

Olesja Starkova: Conceptualization, Formal analysis, Investigation, Writing – original draft. **Sergejs Gaidukovs:** Formal analysis, Methodology, Writing – review & editing. **Oskars Platnieks:** Formal analysis, Investigation, Writing – original draft. **Anda Barkane:** Investigation. **Kristina Garkusina:** Investigation. **Eriks Palitis:** Investigation. **Liga Grase:** Investigation.

Acknowledgements

The study has received funding from M-ERA.Net project NANO2COM “Advanced polymer composites filled with novel 2D nanoparticles”, No. 1.1.1.5/ERANET/18/02 and the Latvian Council of Science project No. lzp-2020/2-0207.

Supplementary materials

Supplementary material associated with this article can be found, in the online version, at doi:10.1016/j.polymdegradstab.2021.109670.

References

[1] P. Jojibabu, Y.X. Zhang, B.G. Prusty, A review of research advances in epoxy-based nanocomposites as adhesive materials, Int. J. Adhes. Adhes. 96 (2020) 102454.
[2] J.M. Sousa, J.R. Correia, S. Cabral-Fonseca, Durability of an epoxy adhesive used in civil structural applications, Constr. Build. Mater. 161 (2018) 618–633.
[3] P. Jojibabu, G.D.J. Ram, A.P. Deshpande, S.R. Bakshi, Effect of carbon nano-filler addition on the degradation of epoxy adhesive joints subjected to hygrothermal aging, Polym. Degrad. Stabil. 140 (2017) 84–94.
[4] G. Scarselli, C. Corcione, F. Nicassio, A. Maffezzoli, Adhesive joints with improved mechanical properties for aerospace applications, Int. J. Adhes. Adhes. 75 (2017) 174–180.
[5] A.F. Abdelkader, J.R. White, Water absorption in epoxy resins: the effects of the crosslinking agent and curing temperature, J. Appl. Polym. Sci. 98 (2005) 2544–2549.
[6] X.F. Sanchez-Romate, P. Teran, S.G. Prolongo, M. Sanchez, A. Urena, Hydrothermal ageing on self-sensing bonded joints with novel carbon nanomaterial reinforced adhesive films, Polym. Degrad. Stabil. 177 (2020) 109170.
[7] O. Starkova, S. Chandrasekaran, T. Schnoor, J. Sevcenko, K. Schulte, Anomalous water diffusion in epoxy/carbon nanoparticle composites, Polym. Degrad. Stabil. 164 (2019) 127–135.
[8] M. Frigione, M. Lettieri, F. Lionetto, L. Mascia, Experimental cold-cured nanostructured epoxy-based hybrid formulations: properties and durability performance, Polymers 12 (2020) 476.
[9] A.E. Krauklis, A.T. Echtermeyer, Mechanism of yellowing: carbonyl formation during hygrothermal aging in a common amine epoxy, Polymers 10 (2018) 1017.
[10] S.A. Grammatikos, B. Zafari, M.C. Evernden, J.T. Mottram, J.M. Mitchels, Moisture uptake characteristics of a pultruded fibre reinforced polymer flat sheet subjected to hot/wet aging, Polym. Degrad. Stabil. 121 (2015) 407–419.
[11] X. Colin, Nonempirical kinetic modeling of non-Fickian water absorption induced by a chemical reaction in epoxy-amine networks, in: P. Davies, Y.D.S. Rajapakse (Eds.), Durability of Composites in a Marine Environment 2, Springer International Publishing AG, 2018, pp. 1–18. (Eds).
[12] G.Z. Xiao, M.E.R. Shanahan, Irreversible effects of hygrothermal aging on DGEBA/DDA epoxy resin, J. Appl. Polym. Sci. 69 (1998) 363–369.
[13] G. Capiel, J. Uicich, D. Fasce, P.E. Montemartini, Diffusion and hydrolysis effects during water aging on an epoxy-anhydride system, Polym. Degrad. Stabil. 153 (2018) 165–171.
[14] J.E. Yagoubi, G. Lubineau, A. Traidia, J. Verdu, Monitoring and simulations of hydrolysis in epoxy matrix composites during hygrothermal aging, Compos. Part B – Eng. 68 (2015) 184–192.
[15] X. Yin, Y. Liu, Y. Miao, G. Xian, Water absorption, hydrothermal expansion, and thermomechanical properties of a vinylester resin for fiber-reinforced polymer composites subjected to water or alkaline solution immersion, Polymers 11 (2019) 505.
[16] T. Glaskova-Kuzmina, A. Aniskevich, G. Papanicolaou, D. Portan, A. Zotti, A. Borriello, M. Zarrelli, Hydrothermal aging of an epoxy resin filled with carbon nanofillers, Polymers 12 (2020) 1153.
[17] A.N. Fraga, V.A. Alvarez, A. Vazquez, Relationship between dynamic mechanical properties and water absorption of unsaturated polyester and vinyl ester glass fiber composites, J. Compos. Mater. 37 (17) (2003).
[18] A. Guen-Geffroy, P.Y. Le Gac, B. Habert, P. Davies, Physical ageing of epoxy in a wet environment: coupling between plasticization and physical ageing, Polym. Degrad. Stabil. 168 (2019) 108947.
[19] A.E. Krauklis, A.G. Akulichev, A. Gagani, A.T. Echtermeyer, Time–temperature—plasticization superposition principle: predicting creep of a plasticized epoxy, Polymers 11 (2019) 1848.
[20] A.E. Krauklis, A.I. Gagani, A.T. Echtermeyer, Long-term hydrolytic degradation of the sizing-rich composite interphase, Coatings 9 (2019) 263.
[21] R. Leger, A. Roy, J.C. Grandidier, Non-classical water diffusion in an industrial adhesive, Int. J. Adhes. Adhes. 30 (2010) 744–753.
[22] D. Gibhardt, A. Doblies, L. Meyer, B. Fiedler, Effects of hygrothermal ageing on the interphase, fatigue, and mechanical properties of glass fibre reinforced epoxy, Fibers 7 (6) (2019) 55.
[23] Q. Deshoulles, M. Le Gall, C. Dreanno, M. Arhant, D. Priour, P.-Y. Le Gac, Modelling pure polyamide 6 hydrolysis: Influence of water content in the amorphous phase, Polym. Degrad. Stabil. 183 (2021) 109435.
[24] O. Starkova, S. Chandrasekaran, P. Lasa, F. Tölle, R. Mülhaupt, K. Schulte, Hydrothermally resistant thermally reduced graphene oxide and multi-wall carbon nanotube based epoxy nanocomposites, Polym. Degrad. Stabil. 98 (2013) 519–526.
[25] S.G. Prolongo, A. Jiménez-Suárez, R. Moriche, A. Ureña, Influence of thickness and lateral size of graphene nanoplatelets on water uptake in epoxy/graphene nanocomposites, Appl. Sci. 8 (2018) 1550.
[26] C. Arribas, M.G. Prolongo, M. Sánchez-Cabezudo, R. Moriche, S.G. Prolongo, Hydrothermal ageing of graphene/carbon nanotubes/epoxy hybrid nanocomposites, Polym. Degrad. Stabil. 170 (2019) 109003.
[27] J.M. Tomasi, I.D. Helman, W.A. Pisani, D.R. Klimek-McDonald, S. Chinkanjanarot, I. Miskioglu, J.A. King, G.M. Odegard, Accelerated hydrothermal aging of cycloaliphatic epoxy/graphene nanoparticle composites, Polym. Degrad. Stabil. 133 (2016) 131–135.
[28] B. Shen, W. Zhai, M. Tao, D. Lu, W. Zheng, Chemical functionalization of graphene oxide toward the tailoring of the interface in polymer composites, Compos. Sci. Technol. 77 (22) (2013) 87–94.
[29] Y.J. Wan, L.X. Gong, L.C. Tang, L.B. Wu, J.X. Jiang, Mechanical properties of epoxy composites filled with silane-functionalized graphene oxide, Compos. Part A – Appl. S 64 (2014) 79–89.
[30] H. Ribeiro, W.M. da Silva, J.C. Neves, H.D.R. Calado, R. Paniago, L.M. Seara, D.M. Camarano, G.G. Silva, Multifunctional nanocomposites based on tetraethylenepentamine-modified graphene oxide/epoxy, Polym. Test 43 (2015) 182–192.
[31] M. Naebe, J. Wang, A. Amini, H. Khayyam, N. Hameed, L.H. Li, Y. Chen, B. Fox, Mechanical property and structure of covalent functionalised graphene/epoxy nanocomposites, Sci. Rep.-Uk 4 (2014) 4375.
[32] Y. Ye, D. Yang, D. Zhang, H. Chen, H. Zhao, X. Lia, L. Wang, POSS-tetraaniline modified graphene for active corrosion protection of epoxy-based organic coating, Chem. Eng. J. 383 (2020) 123160.
[33] L. Li, X. Liao, X. Sheng, P. Liu, Z. Hao, L. He, G. Qin, Influence of surface modified graphene oxide on the mechanical performance and curing kinetics of epoxy resin, Polym. Adv. Technol. 31 (2020) 1865–1874.
[34] S. Amrollahi, B. Ramezanzadeh, H. Yari, M. Ramezanzadeh, M. Mahdavian, Synthesis of polyaniline-modified graphene oxide for obtaining a high performance epoxy nanocomposite film with excellent UV blocking/anti-oxidant/anti-corrosion capabilities, Compos. Part B – Eng. 173 (2019) 106804.
[35] Y.H. Ding, P. Zhang, Q. Zhuo, H.M. Ren, Z.M. Yang, Y. Jiang, A green approach to the synthesis of reduced graphene oxide nanosheets under UV irradiation, Nanotechnology 22 (2011) 215601.
[36] N.I. Zaaba, K.L. Foo, U. Hashim, S.J. Tan, W.W. Liu, C.H. Voon, Synthesis of graphene oxide using modified hummers method: solvent influence, Proc. Eng. 184 (2017) 469–477.
[37] N. Alzate-Carvajal, E.V. Basiuk, V. Meza-Laguna, I. Puente-Lee, M.H. Farıas, N. Bogdanchikova, V.A. Basiuk, Solvent-free one-step covalent functionalization of graphene oxide and nanodiamond with amines, RSC Adv. 6 (2016) 113596.
[38] A. Bouibed, R. Doufnoune, Synthesis and characterization of hybrid materials based on graphene oxide and silica nanoparticles and their effect on the corrosion protection properties of epoxy resin coatings, J. Adhes. Sci. Technol. (2019).
[39] A. Pirayesh, M. Salami-Kalajahi, H. Roghani-Mamaqani, E. Dehghani, Amine–modified graphene oxide as co-curing agent of epoxidized polysulfide prepolymer: thermophysical and mechanical properties of nanocomposites, Diam. Relat. Mater. 86 (2018) 109–116.
[40] R.J.J. Riobo, E. Climent-Pascual, X. Dzez-Betriu, F. Jimenez-Villacorta, C. Prieto, A. de Andres, Elastic constants of graphene oxide few-layer films: correlations with interlayer stacking and bonding, J. Mater. Chem. C 3 (2015) 4868–4875.
[41] J. Crank, The mathematics of diffusion, Clarendon Press, Oxford, 1956.
[42] O. Starkova, S.T. Buschhorn, E. Mannov, K. Schulte, A. Aniskevich, Water transport in epoxy/MWCNT composites, Eur. Polym. 49 (2013) 2138–2148.
[43] M.E.R. Shanahan, Y. Auriac, Water absorption and leaching effects in cellulose diacetate, Polymer 39 (5) (1998) 1155–1164.

[44] L.R. Bao, A.F. Yee, C.Y.C. Lee, Moisture absorption and hygrothermal aging in a bismaleimide resin, Polymer 42 (2001) 7327–7333.
[45] L. Li, Y. Yu, Q. Wu, G. Zhan, S. Li, Effect of chemical structure on the water sorption of amine-cured epoxy resins, Corros. Sci. 51 (2009) 3000–3006.
[46] J. Zhou, J.P. Lucas, Hygrothermal effects of epoxy resin. Part I: the nature of water in epoxy, Polymer 40 (1999) 5505–5512.
[47] F.X. Perrin, M.H. Nguyen, J.L. Vernet, Water transport in epoxy-aliphatic amine networks – Influence of curing cycles, Eur. Polym. J. 45 (2009) 1524–1534.
[48] G.E. Guloglu, M. Cengiz Altan, Moisture absorption of carbon/epoxy nanocomposites, J. Compos. Sci. 4 (2020) 21.
[49] S. Morsch, Y. Liu, S.B. Lyon, S.R. Gibbon, B. Gabriele, M. Malanin, K.J. Eichhorn, Examining the early stages of thermal oxidative degradation in epoxy-amine resins, Polym. Degrad. Stabil. 176 (2020) 109147.
[50] F. Contu, L. Fenzy, S.R. Taylor, An FT-IR investigation of epoxy coatings as a function of electrolyte composition, Prog. Org. Coat. 75 (2012) 92–96.
[51] C.S. Wu, Y.L. Liu, K.Y. Hsu, Maleimide-epoxy resins: preparation, thermal properties, and flame retardance, Polymer 44 (2003) 565–573.
[52] L. Cozzarini, L. Marsich, A. Ferluga, C. Schmid, Failure investigation of a protective epoxy coating by means of crosscheck between infrared spectroscopy and thermal analysis, Eng. Fail. Anal. 107 (2020) 104201.
[53] Z. Deng, M. Wang, C. Zhu, C. Li, J. Liu, M. Tu, L. Xie, D. Gui, Study on light aging of anhydride-cured epoxy resin used for RGB LED packaging material, Polym. Test. 80 (2019) 106131.
[54] J. Jyoti, B. Pratap Singh, A.K. Arya, S.R. Dhakate, Dynamic mechanical properties of multiwall carbon nanotube reinforced ABS composites and their correlation with entanglement density, adhesion, reinforcement and C factor, RSC Adv. 6 (2016) 3997.
[55] L.A. Pothan, Z. Z. Oommen, S. Thomas, Dynamic mechanical analysis of banana fiber reinforced polyester composites, Compos. Sci. Technol. 63 (2003) 283–293.
[56] A. Montazeri, A. Khavandi, J. Javadpour, A. Tcharkhtchi, Viscoelastic properties of multi-walled carbon nanotube/epoxy composites using two different curing cycles, Mater. Design 31 (2010) 3383–3388.
[57] X. Xu, S.H.R. Sanei, E. Steinmetz, A. Gohn, J. Williams, Effect of microstructure uncertainty and testing frequency on storage and loss moduli of injection molded MWCNT reinforced polyamide 66 nanocomposites, Polym. Test. 85 (2020) 106455.
[58] C. Gómez-Navarro, M. Burghard, K. Kern, Elastic properties of chemically derived single graphene sheets, Nano Lett. 8 (2008) 2045–2049.
[59] J. Feng, Z. Guo, Temperature-frequency-dependent mechanical properties model of epoxy resin and its composites, Compos. Part B - Eng. 85 (2016) 161–169.
[60] O.V. Startsev, Y.M. Vapirov, M.P. Lebedev, A.K. Kychkin, Comparison of glass–transition temperatures for epoxy polymers obtained by methods of thermal analysis, Mesh. Compos. Mater. 56 (2) (2020) 227–240.
[61] V.M. Karbhari, Q. Wang, Multi-frequency dynamic mechanical thermal analysis of moisture uptake in E-glass/vinylester composites, Compos. Part B – Eng. 35 (2004) 299–304.
[62] W.K. Goertzen, M.R. Kessler, Creep behavior of carbon fiber/epoxy matrix composites, Mat. Sci. Eng. A - Struct. 421 (2006) 217–225.
[63] H. Li, Y. Luo, D. Hu, D. Jiang, Effect of hydrothermal aging on the dynamic mechanical performance of the room temperature-cured epoxy adhesive, Rheol. Acta 8 (2019) 9–19 5.
[64] A. Plota, A. Masek, Lifetime prediction methods for degradable polymeric materials—a short review, Materials 13 (2020) 4507.
[65] M.G. Prolongo, C. Salom, C. Arribas, M. Sanchez-Cabezudo, R.M. Masegosa, S.G. Prolongo, Influence of graphene nanoplatelets on curing and mechanical properties of graphene/epoxy nanocomposites, J. Therm. Anal. Calorim. 125 (2016) 629–636.